Available online at www.sciencedirect.com
SCIENCE DIRECT®
ELSEVIER
International Journal of Solids and Structures 42 (2005) 5224–5242
INTERNATIONAL JOURNAL OF SOLIDS and STRUCTURES
www.elsevier.com/locate/ijsolstr

A comprehensive analysis of functionally graded sandwich plates: Part 1—Deflection and stresses

A.M. Zenkour *

Department of Mathematics, Faculty of Education, Tanta University, Kafr El-Sheikh 33516, Egypt

Received 12 June 2004; received in revised form 10 February 2005
Available online 13 April 2005

Abstract

A two-dimensional solution is presented for bending analysis of simply supported functionally graded ceramic–metal sandwich plates. The sandwich plate faces are assumed to have isotropic, two-constituent material distribution through the thickness, and the modulus of elasticity and Poisson's ratio of the faces are assumed to vary according to a power-law distribution in terms of the volume fractions of the constituents. The core layer is still homogeneous and made of an isotropic ceramic material. Several kinds of sandwich plates are used taking into account the symmetry of the plate and the thickness of each layer. We derive field equations for functionally graded sandwich plates whose deformations are governed by either the shear deformation theories or the classical theory. Displacement functions that identically satisfy boundary conditions are used to reduce the governing equations to a set of coupled ordinary differential equations with variable coefficients. Numerical results of the sinusoidal, third-order, first-order and classical theories are presented to show the effect of material distribution on the deflections and stresses.

Keywords: Functionally graded material; Sandwich plate; Deflection and stresses; Sinusoidal theory

1. Introduction

Laminated composite materials are commonly used in many kinds of engineering structures. In conventional laminated composite structures, homogeneous elastic laminae are bonded together to obtain enhanced mechanical properties. However, the abrupt change in material properties across the interface between different materials can result in large interlaminar stresses leading to delamination. One way to overcome these adverse effects is to use "functionally graded materials (FGMs)" in which material

* Tel.: +20 473238907; fax: +20 473223415.
E-mail address: zenkour@powernet.com.eg

0020-7683/$ - see front matter © 2005 Elsevier Ltd. All rights reserved.
doi:10.1016/j.ijsolstr.2005.02.015

properties vary continuously. This may be achieved by gradually changing the volume fraction of the constituent materials, usually in the thickness direction only. This eliminates interface problems of composite materials and thus the stress distributions are smooth.

In recent years, FGMs have gained considerable attention as a potential structural material for future high-speed spacecraft and power generation industries. FGMs are composite materials, microscopically inhomogeneous, in which the mechanical properties vary smoothly and continuously from one surface to the other. This is achieved by gradually varying the volume fraction of the constituent materials. This continuous change in composition results in graded properties of FGMs. In an FGM, the composition and structure gradually change over volume, resulting in corresponding changes in the properties of the material. By applying many possibilities inherent in the FGM concept, it is anticipated that materials will be improved and new functions for them created. These novel materials were first introduced by a group of Japanese scientists in 1984 (Yamanouchi et al., 1990; Koizumi, 1993).

In the simplest FGMs, two different material ingredients change gradually from one to the other. Discontinuous changes such as a stepwise gradation of the material ingredients can also be considered an FGM. The most familiar FGM is compositionally graded from a refractory ceramic to a metal. Typically, FGMs are made from a mixture of ceramic and metal or a combination of different materials. The ceramic in an FGM offers thermal barrier effects and protects the metal from corrosion and oxidation, and the FGM is toughened and strengthened by the metallic composition. FGMs are now developed for general use as structural elements in extremely high temperature environments and different applications.

Several studies have been performed to analyze the behaviour of FG structures (Fukui and Yamanaka, 1992; Obata et al., 1992; Noda and Jin, 1993; Fukui et al., 1993; Obata and Noda, 1993, 1994; Jin and Batra, 1996). Reiter et al. (1997) and Reiter and Dvorak (1998) have performed detailed finite element studies of discrete models containing simulated particulate and skeletal microstructures and compared results with those computed from homogenized models in which effective properties were derived by the Mori–Tanaka and the self-consistent methods. Lee and Yu (1998) and Lee et al. (1999) have expanded the mechanical displacements, electric potential and the material moduli as power series in the thickness coordinate and derived plate equations of different orders for FG piezoelectric disks, infinite plates and strips. The response of FG ceramic–metal plates has been investigated by Praveen and Reddy (1998) using a plate finite element that accounts for the transverse shear strains, rotatory inertia and moderately large rotations in von Kármán sense. Reddy and Chin (1998) have studied the dynamic thermoelastic response of FG cylinders and plates. Loy et al. (1999) have studied the vibration of FG cylindrical shells using Love's shell theory. Reddy (2000) has presented solutions for FG rectangular plates based on his third-order shear deformation plate theory.

Cheng and Batra (2000a) have related the deflections of a simply supported FG polygonal plate given by the first-order shear deformation theory and a third-order shear deformation theory to that of an equivalent homogeneous Kirchhoff plate. Cheng and Batra (2000b) have also presented results for the buckling and steady state vibrations of a simply supported FG polygonal plate based on Reddy's plate theory. Analytical 3D solutions for plates are useful since they provide benchmark results to assess the accuracy of various 2D plate theories and finite element formulations. Cheng and Batra (2000c) have also used the method of asymptotic expansion to study the 3D thermoelastic deformations of an FG elliptic plate. Recently, Vel and Batra (2002) have presented an exact 3D solution for the thermoelastic deformation of FG simply supported plates of finite dimensions.

In general, FG plates do not have material properties symmetric about the mid-plane. Therefore, their stretching and bending deformation modes are coupled. This, however, is not the case for plates or beams symmetric about the mid-plane (Zenkour, 1999). The primary objective of this paper is to present a general formulation for FG sandwich plates using the sinusoidal shear deformation plate theory of Zenkour (2004a,b,c, 2005). The plate may be symmetric about the mid-plane and made from three layers. The face layers are assumed to be ceramic–metal FGMs whereas the core layer is considered as a homogeneous

ceramic material. As a special case, a non-symmetric FGM sandwich plate is presented. Deflections and stresses of FGM sandwich plates are investigated using sinusoidal plate theory. Results for the classical plate theory, the first-order and third-order shear deformation plate theories can also be obtained from the present analysis.

2. Problem formulation

Let us consider the case of a flat sandwich plate composed of three microscopically heterogeneous layers as shown in Fig. 1. Rectangular Cartesian coordinates x_i are used to describe infinitesimal deformations of a three-layer sandwich elastic plate occupying the region $[0,a]\times[0,b]\times[-h/2,+h/2]$ in the unstressed reference configuration. The mid-plane of the composite sandwich plate is defined by $x_3=0$ and its external bounding planes being defined by $x_3=\pm h/2$ while x_α denote the in-plane coordinates. For the sake of compactness, the equations will be derived in tensorial notations and specialized afterwards for the problem under consideration. Partial differentiation will be denoted by a comma, i.e. $(\,)_{,i}=\partial(\,)/\partial x_i$. The Einsteinian summation convention will be used with Latin indices ranging from 1 to 3 and Greek indices ranging from 1 to 2.

The face layers of the sandwich plate are made of an isotropic material with material properties varying smoothly in the x_3 (thickness) direction only. The core layer is made of an isotropic homogeneous material. The vertical positions of the bottom and top, and of the two interfaces between the layers are denoted by $h_0=-h/2$, h_1, h_2, $h_3=h/2$. The effective material properties for each layer, like Young's modulus and Poisson's ratio, can be expressed as

$$P(x_3)=P_{\mathrm{m}}+(P_{\mathrm{c}}-P_{\mathrm{m}})V^{(n)}, \tag{1}$$

where P_{m} and P_{c} denote the property of the bottom and top faces of layer 1, respectively, and vice versa for layer 3 depending on the volume fraction $V^{(n)}$ ($n=1,2,3$). Note that P_{m} and P_{c} are, respectively, the corresponding properties of the metal and ceramic of the FGM sandwich plate. The volume fraction $V^{(n)}$

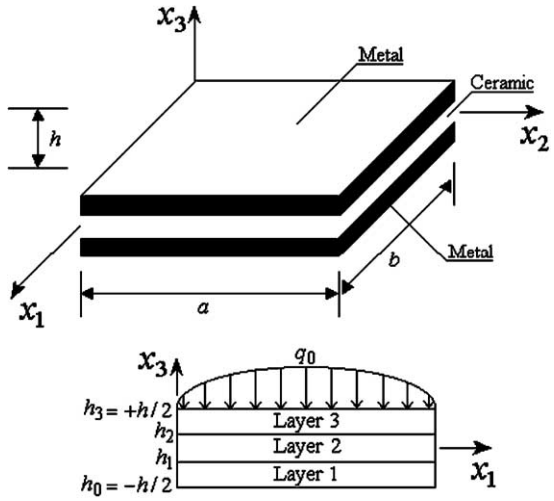

Fig. 1. Geometry of the FGM sandwich rectangular plate.

through the thickness of the sandwich plate faces follows a simple power-law while it equals unity in the core layer. It reads

$$V^{(1)} = \left(\frac{x_3 - h_0}{h_1 - h_0}\right)^k, \quad x_3 \in [h_0, h_1], \tag{2a}$$

$$V^{(2)} = 1, \quad x_3 \in [h_1, h_2], \tag{2b}$$

$$V^{(3)} = \left(\frac{x_3 - h_3}{h_2 - h_3}\right)^k, \quad x_3 \in [h_2, h_3], \tag{2c}$$

where k is a parameter that dictates the material variation profile through the faces thickness (the volume fraction exponent), which takes values greater than or equal to zero. The core layer is independent of the value of k which is a fully ceramic layer. However, the value of k equal to zero represents a fully ceramic plate. The above power-law assumption given in Eqs. (2a) and (2c) reflects a simple rule of mixtures used to obtain the effective properties of the ceramic–metal plate faces (see Fig. 1). Note that the volume fraction of the metal is high near the bottom and top surfaces of the plate, and that of ceramic high near the interfaces. In addition, Eq. (2) indicates that the top and bottom surfaces of the plate are metal-rich whereas the bottom ($x_3 = h_1$) and top ($x_3 = h_2$) surfaces of the core are ceramic-rich.

The displacements of a material point located at (x_1, x_2, x_3) in the plate may be written as (Zenkour, 2004a,b,c, 2005)

$$\left.\begin{aligned} v_\alpha(x_i) &= u_\alpha - x_3 u_{3,\alpha} + \Psi\varphi_\alpha, \\ v_3(x_i) &= u_3, \end{aligned}\right\} \tag{3}$$

where u_α, u_3 and φ_α are independent of x_3 and denote the displacements and rotations of transverse normal on the plane $x_3 = 0$, respectively. The displacement of the classical thin plate theory (CLPT) is obtained easily by setting $\Psi(x_3) = 0$. The displacement of the first-order shear deformation plate theory (FSDPT) is obtained by setting $\Psi(x_3) = x_3$. Also, the displacement of the third-order shear deformation plate theory (TSDPT) of Reddy (2000) is obtained by setting

$$\Psi(x_3) = x_3\left[1 - \frac{4}{3}\left(\frac{x_3}{h}\right)^2\right]. \tag{4}$$

In addition, the sinusoidal shear deformation plate theory (SSDPT) of Zenkour (2004a,b,c, 2005) is obtained by setting

$$\Psi(x_3) = \frac{h}{\pi}\sin\left(\frac{\pi x_3}{h}\right). \tag{5}$$

The present SSDPT is simplified by enforcing traction-free boundary conditions at the plate faces. It contains the same dependent unknowns as first- and third-order shear deformation theories, but accounts according to cosine-law distribution of the transverse shear strains through the thickness of the plate. No transverse shear correction factors are needed for both SSDPT and TSDPT because a correct representation of the transverse shearing strain is given.

Consistent with Eq. (3), the six strain components compatible with the displacement field display the form:

$$\begin{aligned} e_{\alpha\beta} &= \varepsilon_{\alpha\beta} + x_3\kappa_{\alpha\beta} + \Psi\eta_{\alpha\beta}, \\ e_{\alpha 3} &= \Psi_{,3}\varepsilon_{\alpha 3}, \\ e_{33} &= 0. \end{aligned} \tag{6}$$

Here the non-vanishing strain measures $e_{ij} \equiv e_{ij}(x_\omega)$ are expressed in terms of the displacement quantities as

$$\begin{aligned}
\varepsilon_{\alpha\beta} &= \frac{1}{2}(u_{\alpha,\beta} + u_{\beta,\alpha}),\\
\kappa_{\alpha\beta} &= -u_{3,\alpha\beta},\\
\eta_{\alpha\beta} &= \frac{1}{2}(\varphi_{\alpha,\beta} + \varphi_{\beta,\alpha}),\\
\varepsilon_{\alpha 3} &= \frac{1}{2}\varphi_\alpha.
\end{aligned} \tag{7}$$

The stress–strain relationships accounting for transverse shear deformation in the plate coordinates, can be expressed as

$$\sigma^{(n)}_{\alpha\beta} = H^{(n)}_{\alpha\beta\omega\rho} e_{\omega\rho}, \qquad \sigma^{(n)}_{\alpha 3} = 2E^{(n)}_{\alpha 3\omega 3} e_{\omega 3}, \tag{8}$$

where $H^{(n)}_{\alpha\beta\omega\rho}$ and $E^{(n)}_{\alpha 3\omega 3}$ are the components of the elasticity tensor for a transversely-isotropic material of layer n with the plane of isotropy x_1–x_2,

$$\begin{aligned}
H^{(n)}_{\alpha\beta\omega\rho} &= \frac{\nu_{(n)}E_{(n)}}{1-\nu^2_{(n)}}\delta_{\alpha\beta}\delta_{\omega\rho} + G'_{(n)}(\delta_{\alpha\omega}\delta_{\beta\rho} + \delta_{\alpha\rho}\delta_{\beta\omega}),\\
E^{(n)}_{\alpha 3\omega 3} &= G'_{(n)}\delta_{\alpha\omega},
\end{aligned} \tag{9}$$

in which $E_{(n)}(x_3)$ and $\nu_{(n)}(x_3)$ are Young's modulus and Poisson's ratio characterizing elastic properties in the plane of isotropy of the nth layer and $\delta_{\alpha\beta}$ is Kronecker's delta. The shear modulus $G_{(n)}$ characterizing the material response under a shear load applied in the plane of isotropy, takes the form

$$G_{(n)}(x_3) = \frac{E_{(n)}}{2(1+\nu_{(n)})}, \tag{10}$$

while $G'_{(n)}(x_3)$ is the shear modulus in the plane perpendicular to the plane of isotropy. It is to be noted that $G'_{(n)} = G_{(n)}$ for an isotropic layer.

The principle of virtual work in the present case yields

$$\int_{-h/2}^{h/2}\int_\Omega \left[\sigma^{(n)}_{11}\delta e_{11} + \sigma^{(n)}_{22}\delta e_{22} + \cdots\right] \mathrm{d}\Omega\,\mathrm{d}x_3 - \int_\Omega q\delta u_3\,\mathrm{d}\Omega = 0, \tag{11}$$

or

$$\begin{aligned}
\int_\Omega [&N_{11}\delta\varepsilon_{11} + 2N_{12}\delta\varepsilon_{12} + N_{22}\delta\varepsilon_{22} + M_{11}\delta\kappa_{11} + 2M_{12}\delta\kappa_{21} + M_{22}\delta\kappa_{22} + 2Q_{13}\delta\varepsilon_{13} + 2Q_{23}\delta\varepsilon_{23} + S_{11}\delta\eta_{11}\\
&+2S_{12}\delta\eta_{12} + S_{22}\delta\eta_{22} - q\delta u_3]\mathrm{d}\Omega = 0,
\end{aligned} \tag{12}$$

where $N_{\alpha\beta}$ and $M_{\alpha\beta}$ are the basic components of stress resultants and stress couples; $S_{\alpha\beta}$ are additional stress couples associated with the transverse shear effects; and $Q_{\alpha 3}$ are transverse shear stress resultants. They can expressed as

$$(N_{\alpha\beta}, M_{\alpha\beta}, S_{\alpha\beta}) = \sum_{n=1}^{3}\int_{h_{n-1}}^{h_n}(1, x_3, \Psi)\sigma^{(n)}_{\alpha\beta}\,\mathrm{d}x_3, \tag{13a}$$

$$Q_{\alpha 3} = \sum_{n=1}^{3}\int_{h_{n-1}}^{h_n}\Psi_{,3}\sigma^{(n)}_{\alpha 3}\,\mathrm{d}x_3. \tag{13b}$$

Here h_n and h_{n-1} are the top and bottom x_3-coordinates of the nth lamina.

3. Governing equations

The governing equations of equilibrium can be derived from Eq. (12) by integrating the displacement gradients in e_{ij} by parts and setting the coefficients δu_i and $\delta\varphi_\alpha$ to zero separately. Thus one can obtain

$$N_{\alpha\beta,\beta}=0,\quad M_{\alpha\beta,\alpha\beta}+q=0,\quad S_{\alpha\beta,\beta}-Q_{\alpha 3}=0. \tag{14}$$

Using Eq. (8) in Eq. (13), the stress resultants can be related to the total strains by

$$\begin{Bmatrix} N_{\alpha\beta}\\ M_{\alpha\beta}\\ S_{\alpha\beta}\end{Bmatrix}=([A]-[B])\begin{Bmatrix}\varepsilon_{11}+\varepsilon_{22}\\ \kappa_{11}+\kappa_{22}\\ \eta_{11}+\eta_{22}\end{Bmatrix}\delta_{\alpha\beta}+[B]\begin{Bmatrix}\varepsilon_{\alpha\beta}\\ \kappa_{\alpha\beta}\\ \eta_{\alpha\beta}\end{Bmatrix},\qquad Q_{\alpha 3}=C\varphi_\alpha, \tag{15}$$

where

$$[A]=\sum_{n=1}^{3}\int_{h_{n-1}}^{h_n}\frac{E_{(n)}}{1-\nu_{(n)}^2}\begin{bmatrix}1 & x_3 & \Psi\\ x_3 & x_3^2 & x_3\Psi\\ \Psi & x_3\Psi & \Psi^2\end{bmatrix}\mathrm{d}x_3, \tag{16a}$$

$$[B]=\sum_{n=1}^{3}\int_{h_{n-1}}^{h_n}\frac{E_{(n)}}{1+\nu_{(n)}}\begin{bmatrix}1 & x_3 & \Psi\\ x_3 & x_3^2 & x_3\Psi\\ \Psi & x_3\Psi & \Psi^2\end{bmatrix}\mathrm{d}x_3, \tag{16b}$$

$$C=\sum_{n=1}^{3}\int_{h_{n-1}}^{h_n}G'_{(n)}(\Psi_{,3})^2\,\mathrm{d}x_3. \tag{16c}$$

Substituting Eq. (15) into Eq. (14), we obtain the following equations for all theories,

SSDPT and TSDPT:

$$A^{11}u_{1,11}+\frac{1}{2}B^{11}u_{1,22}+\left(A^{11}-\frac{1}{2}B^{11}\right)u_{2,12}-A^{12}\nabla^2u_{3,1}+A^{13}\varphi_{1,11}+\frac{1}{2}B^{13}\varphi_{1,22}+\left(A^{13}-\frac{1}{2}B^{13}\right)\varphi_{2,12}=0,\quad(1\leftrightarrow 2), \tag{17a}$$

$$A^{12}\left(\nabla^2u_{1,1}+\nabla^2u_{2,2}\right)-A^{22}\nabla^4u_3+A^{23}\left(\nabla^2\varphi_{1,1}+\nabla^2\varphi_{2,2}\right)+q=0, \tag{17b}$$

$$A^{13}u_{1,11}+\frac{1}{2}B^{13}u_{1,22}+\left(A^{13}-\frac{1}{2}B^{13}\right)u_{2,12}-A^{23}\nabla^2u_{3,1}+A^{33}\varphi_{1,11}+\frac{1}{2}B^{33}\varphi_{1,22}+\left(A^{33}-\frac{1}{2}B^{33}\right)\varphi_{2,12}-C\varphi_1=0,\quad(1\leftrightarrow 2), \tag{17c}$$

where A^{ij} and B^{ij} are the elements of the symmetric matrices $[A]$ and $[B]$, respectively. In addition, the sign $(1\leftrightarrow 2)$ indicates that from Eqs. (17a) and (17c) other equations may be obtained by interchanging the sub-index 1 by 2 and vice versa and $\nabla^2(\,)=(\,)_{,11}+(\,)_{,22}$ is *Laplace* operator.

FSDPT:

$$A^{11}(u_{1,1}+u_{2,2})_{,1}+\frac{1}{2}B^{11}(u_{1,2}-u_{2,1})_{,2}+A^{12}\left(\varphi_{1,1}+\varphi_{2,2}-\nabla^2u_3\right)_{,1}+\frac{1}{2}B^{12}(\varphi_{1,2}-\varphi_{2,1})_{,2}=0,\quad(1\leftrightarrow 2), \tag{18a}$$

$$A^{12}\left(\nabla^2 u_{1,1}+\nabla^2 u_{2,2}\right)+A^{22}\left(\nabla^2\varphi_{1,1}+\nabla^2\varphi_{2,2}-\nabla^4 u_3\right)+q=0, \tag{18b}$$

$$A^{12}(u_{1,1}+u_{2,2})_{,1}+\frac{1}{2}B^{12}(u_{1,2}-u_{2,1})_{,2}+A^{22}\left(\varphi_{1,1}+\varphi_{2,2}-\nabla^2 u_3\right)_{,1}+\frac{1}{2}B^{22}(\varphi_{1,2}-\varphi_{2,1})_{,2} - C_F\varphi_1=0, \quad (1\leftrightarrow 2), \tag{18c}$$

where

$$C_F=\sum_{n=1}^{3}\int_{h_{n-1}}^{h_n} KG'_{(n)}\,\mathrm{d}x_3, \tag{19}$$

in which K is the shear correction factor.

CLPT:

$$A^{11}(u_{1,1}+u_{2,2})_{,1}+\frac{1}{2}B^{11}(u_{1,2}-u_{2,1})_{,2}-A^{12}\nabla^2 u_{3,1}=0, \quad (1\leftrightarrow 2), \tag{20a}$$

$$A^{12}(\nabla^2 u_{1,1}+\nabla^2 u_{2,2})-A^{22}\nabla^4 u_3+q=0. \tag{20b}$$

For further computational reasons the converted expressions of the stress components are also recorded. They read

SSDPT:

$$\begin{aligned}
\sigma_{11}^{(n)}&=\frac{E_{(n)}}{1-v_{(n)}^2}\left\{u_{1,1}+v_{(n)}u_{2,2}-x_3\left(u_{3,11}+v_{(n)}u_{3,22}\right)+\frac{h}{\pi}\sin\left(\frac{\pi x_3}{h}\right)\left(\varphi_{1,1}+v_{(n)}\varphi_{2,2}\right)\right\}, \quad (1\leftrightarrow 2),\\
\sigma_{12}^{(n)}&=\frac{E_n}{2(1+v_n)}\left\{u_{1,2}+u_{2,1}-2x_3u_{3,12}+\frac{h}{\pi}\sin\left(\frac{\pi x_3}{h}\right)\left(\varphi_{1,2}+\varphi_{2,1}\right)\right\},\\
\sigma_{13}^{(n)}&=G'_{(n)}\cos\left(\frac{\pi x_3}{h}\right)\varphi_1, \quad (1\leftrightarrow 2).
\end{aligned} \tag{21a}$$

TSDPT:

$$\begin{aligned}
\sigma_{11}^{(n)}&=\frac{E_{(n)}}{1-v_{(n)}^2}\left\{u_{1,1}+v_{(n)}u_{2,2}+x_3\left[(\varphi_1-u_{3,1})_{,1}+v_{(n)}(\varphi_2-u_{3,2})_{,2}\right]-\frac{4}{3}\frac{x_3^3}{h^2}\left(\varphi_{1,1}+v_{(n)}\varphi_{2,2}\right)\right\}, \quad (1\leftrightarrow 2),\\
\sigma_{12}^{(n)}&=\frac{E_n}{2(1+v_n)}\left\{u_{1,2}+u_{2,1}+x_3\left[(\varphi_1-u_{3,1})_{,2}+(\varphi_2-u_{3,2})_{,1}\right]-\frac{4}{3}\frac{x_3^3}{h^2}(\varphi_{1,2}+\varphi_{2,1})\right\},\\
\sigma_{13}^{(n)}&=G'_{(n)}\left[1-4\left(\frac{x_3}{h}\right)^2\right]\varphi_1, \quad (1\leftrightarrow 2).
\end{aligned} \tag{21b}$$

FSDPT:

$$\begin{aligned}
\sigma_{11}^{(n)}&=\frac{E_{(n)}}{1-v_{(n)}^2}\left\{u_{1,1}+v_{(n)}u_{2,2}+x_3\left[(\varphi_1-u_{3,1})_{,1}+v_{(n)}(\varphi_2-u_{3,2})_{,2}\right]\right\}, \quad (1\leftrightarrow 2),\\
\sigma_{12}^{(n)}&=\frac{E_n}{2(1+v_n)}\left\{u_{1,2}+u_{2,1}+x_3\left[(\varphi_1-u_{3,1})_{,2}+(\varphi_2-u_{3,2})_{,1}\right]\right\},\\
\sigma_{13}^{(n)}&=G'_{(n)}\varphi_1, \quad (1\leftrightarrow 2).
\end{aligned} \tag{21c}$$

CLPT:

$$\sigma_{11}^{(n)} = \frac{E_{(n)}}{1-\nu_{(n)}^2}\left\{u_{1,1} + \nu_{(n)}u_{2,2} - x_3\left(u_{3,11} + \nu_{(n)}u_{3,22}\right)\right\}, \quad (1 \leftrightarrow 2),$$
$$\sigma_{12}^{(n)} = \frac{E_n}{2(1+\nu_n)}\{u_{1,2} + u_{2,1} - 2x_3u_{3,12}\}. \tag{21d}$$

4. Exact solutions for FGMs sandwich plates

Rectangular plates are generally classified in accordance with the type of support used. We are here concerned with the exact solutions of Eqs. (17), (18) and (20) for a simply supported FGM plate. The following boundary conditions are imposed at the side edges for the shear deformation theories:

$$\begin{aligned} &u_2 = u_3 = \varphi_2 = N_{11} = M_{11} = S_{11} = 0, \quad \text{at } x_1 = 0, a, \\ &u_1 = u_3 = \varphi_1 = N_{22} = M_{22} = S_{22} = 0, \quad \text{at } x_2 = 0, b. \end{aligned} \tag{22a}$$

For CLPT, the boundary conditions are

$$\begin{aligned} &u_2 = u_3 = N_{11} = M_{11} = 0, \quad \text{at } x_1 = 0, a, \\ &u_1 = u_3 = N_{22} = M_{22} = 0, \quad \text{at } x_2 = 0, b. \end{aligned} \tag{22b}$$

To solve this problem, Navier presented the external force for the case of sinusoidally distributed load as

$$q(x,y) = q_0 \sin(\lambda x)\sin(\mu y), \tag{23}$$

where $\lambda = \pi/a$, $\mu = \pi/b$, and q_0 represents the intensity of the load at the plate center.

Following the Navier solution procedure, we assume the following solution form for $(u_1, u_2, u_3, \varphi_1, \varphi_2)$ that satisfies the boundary conditions,

$$\begin{Bmatrix} u_1 \\ u_2 \\ u_3 \\ \varphi_1 \\ \varphi_2 \end{Bmatrix} = \begin{Bmatrix} U_1\cos(\lambda x)\sin(\mu y) \\ U_2\sin(\lambda x)\cos(\mu y) \\ U_3\sin(\lambda x)\sin(\mu y) \\ \Phi_1\cos(\lambda x)\sin(\mu y) \\ \Phi_2\sin(\lambda x)\cos(\mu y) \end{Bmatrix}, \tag{24}$$

where U_1, U_2, U_3, Φ_1, and Φ_2 are arbitrary parameters to be determined subjected to the condition that the solution in Eq. (24) satisfies the equilibrium equations, Eqs. (17), (18) and (20). Equation (24) is appropriate for CLPT by ignoring the functions φ_1 and φ_2. Substituting Eq. (24) into Eqs. (17), (18) and (20), one obtains

$$[L]\{\Delta\} = \{F\}, \tag{25}$$

where $\{\Delta\}$ and $\{F\}$ denote the columns

$$\begin{aligned} \{\Delta\}^{\mathrm{T}} &= \{U_1, U_2, U_3, \Phi_1, \Phi_2\}, \\ \{F\}^{\mathrm{T}} &= \{0, 0, -q_0, 0, 0\}, \end{aligned} \tag{26}$$

for the shear deformation theories and denote the columns

$$\begin{aligned} \{\Delta\}^{\mathrm{T}} &= \{U_1, U_2, U_3\}, \\ \{F\}^{\mathrm{T}} &= \{0, 0, -q_0\}, \end{aligned} \tag{27}$$

for the CLPT. For all theories the elements $L^{ij} = L^{ji}$ of the coefficient matrix $[L]$ are defined in Appendix A.

5. Several kinds of sandwich plates

Fig. 2 shows the through-the-thickness variation of the volume fraction function of the ceramic for $k = 0.02, 0.2, 1, 2, 5$. Note that the core of the plate is fully ceramic while the bottom and top surfaces of the plate are metal-rich. For constant value of Poisson's ratio $\nu_{(n)} = \nu$, one gets $B^{ij} = (1 - \nu)A^{ij}$. It is to be noted that the coefficients A^{11}, A^{12} and A^{22} are the same for all theories. The other coefficients A^{13}, A^{23} and A^{33} may be vanished for CLPT. For shear deformation theories, these coefficients as well as C and C_F are given directly according to Eqs. (16) and (19).

5.1. (1-2-1) FGM sandwich plate

Here the plate is symmetric, in which the core thickness equals the sum of faces thickness (see Fig. 2a). In this case, we have

$$h_1 = -h/4, \qquad h_2 = h/4. \tag{28}$$

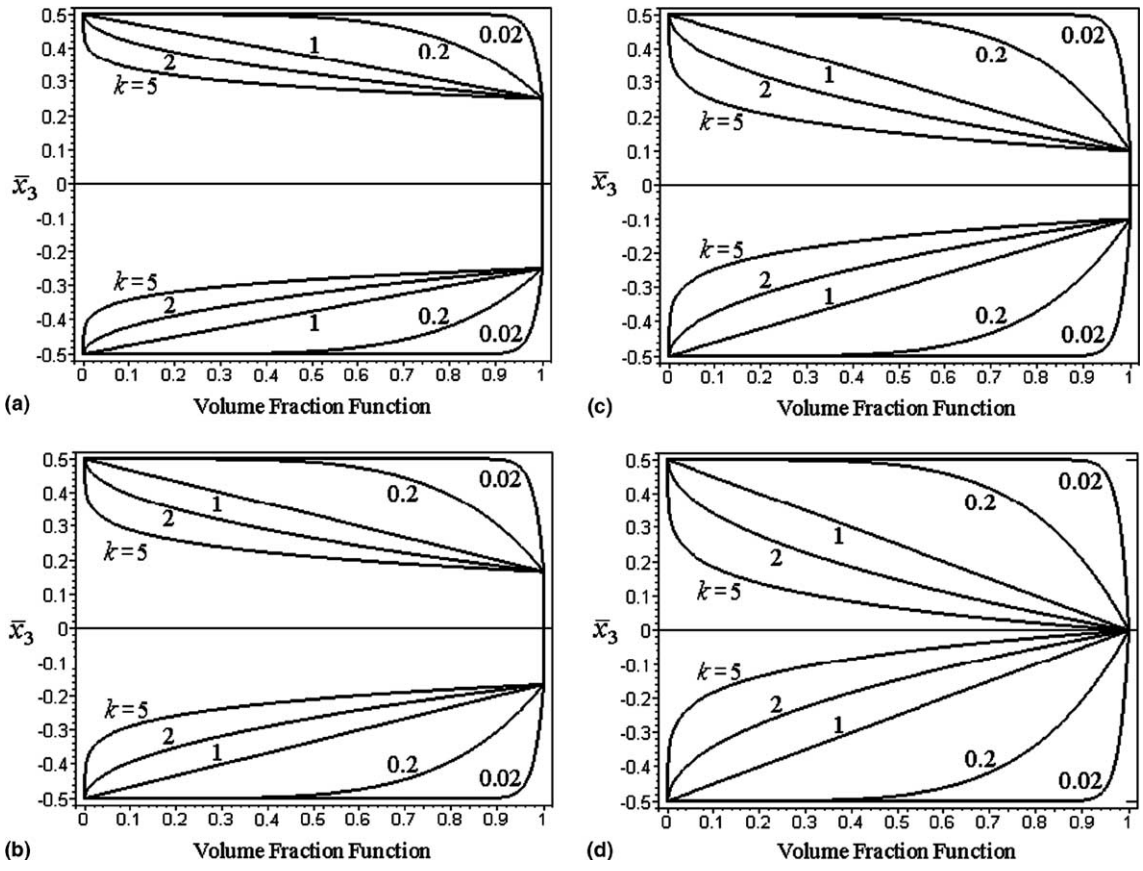

Fig. 2. Variation of volume fraction function through plate thickness for various values of the power-law index k and different types of sandwich plates. (a) The (1-2-1) FGM sandwich plate, (b) The (1-1-1) FGM sandwich plate, (c) The (2-1-2) FGM sandwich plate, (d) The (1-0-1) FGM sandwich plate.

5.2. (1-1-1) FGM sandwich plate

As shown in Fig. 2b the plate is symmetric and made of three equal-thickness layers. So, one takes

$$h_1 = -h/6, \qquad h_2 = h/6. \tag{29}$$

5.3. (2-1-2) FGM sandwich plate

In this case the plate is also symmetric and the thickness of the core is half the face thickness. Fig. 2c shows that

$$h_1 = -h/10, \qquad h_2 = h/10. \tag{30}$$

5.4. (1-0-1) FGM sandwich plate

In this case the plate is symmetric and made of only two equal-thickness layers, i.e. there is no core layer (see Fig. 2d). Thus,

$$h_1 = h_2 = 0. \tag{31}$$

6. Numerical results

The static analysis is conducted for two combinations of metal and ceramic. The first set of materials chosen is aluminum and alumina. The second combination of materials consisted of aluminum and zirconia. The Young's modulus and Poisson's ratio, are for aluminum: 70 GPa, 0.3, alumina: 380 GPa, 0.3, and for zirconia: 151 GPa, 0.3, respectively. For simplicity, Poisson's ratio of aluminum, alumina and zirconia is assigned the same value; it is equivalent to the assumption that the effective value of the shear modulus is also derived from Eq. (1).

Numerical results are presented in terms of non-dimensional stresses and deflection. The various non-dimensional parameters used are

$$\text{center deflection } \bar{u}_3 : \frac{10hE_0}{a^2 q_0} u_3\left(\frac{a}{2}, \frac{b}{2}\right),$$

$$\text{axial stress } \bar{\sigma}_{11} : \frac{10h^2}{a^2 q_0} \sigma_{11}\left(\frac{a}{2}, \frac{b}{2}, \frac{h}{2}\right),$$

$$\text{shear stress } \bar{\sigma}_{13} : \frac{h}{a q_0} \sigma_{13}\left(0, \frac{b}{2}, 0\right),$$

$$\text{thickness coordinate } \bar{x}_3 : \frac{x_3}{h},$$

where the reference value is taken as $E_0 = 1$ GPa. Numerical results are tabulated in Tables 1–4 and plotted in Figs. 3–9. It is assumed (unless otherwise stated) that the plate is made from aluminum–zirconia FGM and $a/h = 10$, $a/b = 1$. The shear correction factor of FSDPT is fixed to be $K = 5/6$.

Table 1
Effects of volume fraction exponent on the dimensionless deflection of the FGM square plate

k	Theory	$\bar{u}_3$				
		1-0-1	2-1-2	1-1-1	2-2-1	1-2-1
0	SSDPT	0.19605	0.19605	0.19605	0.19605	0.19605
	TSDPT	0.19606	0.19606	0.19606	0.19606	0.19606
	FSDPT	0.19607	0.19607	0.19607	0.19607	0.19607
	CLPT	0.18560	0.18560	0.18560	0.18560	0.18560
1	SSDPT	0.32349	0.30624	0.29194	0.28082	0.27093
	TSDPT	0.32358	0.30632	0.29199	0.28085	0.27094
	FSDPT	0.32484	0.30750	0.29301	0.28168	0.27167
	CLPT	0.31054	0.29417	0.28026	0.26920	0.25958
2	SSDPT	0.37319	0.35218	0.33280	0.31611	0.30260
	TSDPT	0.37335	0.35231	0.33289	0.31617	0.30263
	FSDPT	0.37514	0.35408	0.33441	0.31738	0.30370
	CLPT	0.35885	0.33942	0.32067	0.30405	0.29095
5	SSDPT	0.40905	0.39160	0.37128	0.34950	0.33474
	TSDPT	0.40927	0.39183	0.37145	0.34960	0.33480
	FSDPT	0.41120	0.39418	0.37356	0.35123	0.33631
	CLPT	0.39227	0.37789	0.35865	0.33693	0.32283
10	SSDPT	0.41750	0.40376	0.38490	0.34916	0.34119
	TSDPT	0.41772	0.40407	0.38551	0.36215	0.34824
	FSDPT	0.41919	0.40657	0.38787	0.36395	0.34996
	CLPT	0.39876	0.38941	0.37236	0.34915	0.33612

Table 2
Effects of volume fraction exponent on the dimensionless axial stress of the FGM square plate

k	Theory	$\bar{\sigma}_{11}$				
		1-0-1	2-1-2	1-1-1	2-2-1	1-2-1
0	SSDPT	2.05452	2.05452	2.05452	2.05452	2.05452
	TSDPT	2.04985	2.04985	2.04985	2.04985	2.04985
	FSDPT	1.97576	1.97576	1.97576	1.97576	1.97576
1	SSDPT	1.58204	1.49859	1.42892	1.32342	1.32590
	TSDPT	1.57923	1.49587	1.42617	1.32062	1.32309
	FSDPT	1.53245	1.45167	1.38303	1.27749	1.28096
2	SSDPT	1.82450	1.72412	1.63025	1.47387	1.48283
	TSDPT	1.82167	1.72144	1.62748	1.47095	1.47988
	FSDPT	1.77085	1.67496	1.58242	1.42528	1.43580
5	SSDPT	1.99567	1.91547	1.81838	1.61477	1.64106
	TSDPT	1.99272	1.91302	1.81580	1.61181	1.63814
	FSDPT	1.93576	1.86479	1.76988	1.56401	1.59309
10	SSDPT	2.03360	1.97313	1.88147	1.61979	1.64851
	TSDPT	2.03036	1.97126	1.88376	1.66660	1.70417
	FSDPT	1.96780	1.92165	1.83754	1.61645	1.65844

Fig. 3 shows the variation of the center deflection with side-to-thickness ratio for different type of FG symmetric plates. We will present only the significant results or difference in the response of plates with

Table 3
Effects of volume fraction exponent on the dimensionless transverse shear stress of the FGM square plate

k	Theory	$\bar{\sigma}_{13}$				
		1-0-1	2-1-2	1-1-1	2-2-1	1-2-1
0	SSDPT	0.24618	0.24618	0.24618	0.24618	0.24618
	TSDPT	0.23857	0.23857	0.23857	0.23857	0.23857
	FSDPT	0.19099	0.19099	0.19099	0.19099	0.19099
1	SSDPT	0.29907	0.27774	0.26809	0.26680	0.26004
	TSDPT	0.29203	0.27104	0.26117	0.25951	0.25258
	FSDPT	0.26099	0.24316	0.23257	0.22762	0.22057
2	SSDPT	0.33285	0.29422	0.27807	0.27627	0.26543
	TSDPT	0.32622	0.28838	0.27188	0.26939	0.25834
	FSDPT	0.29731	0.26752	0.25077	0.24316	0.23257
5	SSDPT	0.39370	0.31930	0.29150	0.28895	0.27153
	TSDPT	0.38634	0.31454	0.28643	0.28265	0.26512
	FSDPT	0.34538	0.29731	0.27206	0.26099	0.24596
10	SSDPT	0.44147	0.33644	0.29529	0.29671	0.27676
	TSDPT	0.43206	0.33242	0.29566	0.29080	0.26895
	FSDPT	0.37277	0.31316	0.28299	0.26998	0.25257

Table 4
Effects of aspect ratio on the dimensionless deflection of the FGM rectangular plate ($k = 2$)

Scheme	Theory	$\bar{u}_3$				
		$a/b = 1/3$	$a/b = 0.5$	$a/b = 1.0$	$a/b = 1.5$	$a/b = 2.0$
1-0-1	SSDPT	1.18849	0.94160	0.37319	0.14472	0.06315
	TSDPT	1.18877	0.94186	0.37335	0.14481	0.06321
	FSDPT	1.19200	0.94473	0.37514	0.14592	0.06393
	CLPT	1.16267	0.91865	0.35885	0.13590	0.05742
2-1-2	SSDPT	1.12269	0.88933	0.35218	0.13639	0.05941
	TSDPT	1.12293	0.88955	0.35231	0.13647	0.05946
	FSDPT	1.12611	0.89237	0.35408	0.13756	0.06017
	CLPT	1.09971	0.86891	0.33942	0.12854	0.05431
1-1-1	SSDPT	1.06080	0.84032	0.33280	0.12890	0.05615
	TSDPT	1.06096	0.84046	0.33289	0.12895	0.05619
	FSDPT	1.06369	0.84289	0.33441	0.12989	0.05680
	CLPT	1.03895	0.82090	0.32067	0.12144	0.05131
2-2-1	SSDPT	1.00683	0.79767	0.31611	0.12256	0.05347
	TSDPT	1.00694	0.79776	0.31617	0.12260	0.05349
	FSDPT	1.00911	0.79969	0.31738	0.12334	0.05398
	CLPT	0.98512	0.77837	0.30405	0.11514	0.04865
1-2-1	SSDPT	0.96366	0.76348	0.30260	0.11735	0.05121
	TSDPT	0.96371	0.76353	0.30263	0.11737	0.05122
	FSDPT	0.96563	0.76524	0.30370	0.10803	0.05165
	CLPT	0.94269	0.74484	0.29095	0.11018	0.04655

the different material combinations. For both material pairs, the deflection of the metallic plate is found to be of the largest magnitude and that of the ceramic plate, of the smallest magnitude. All the plates with

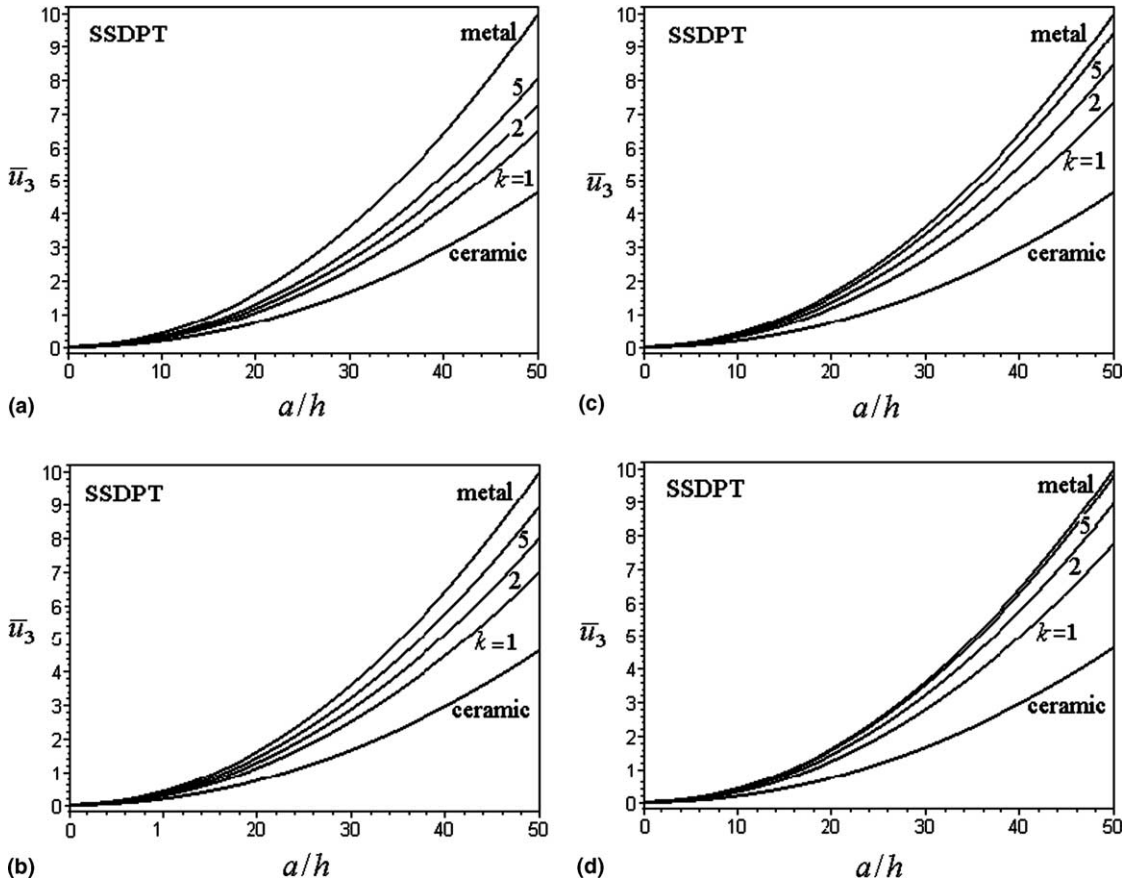

Fig. 3. Dimensionless center deflection ($\bar{u}_3$) as a function of side-to-thickness ratio (a/h) of an FGM sandwich plate for various values of k and different types of sandwich plates. (a) The (1-2-1) FGM sandwich plate. (b) The (1-1-1) FGM sandwich plate. (c) The (2-1-2) FGM sandwich plate. (d) The (1-0-1) FGM sandwich plate.

intermediate properties undergo corresponding intermediate values of center deflection. This is expected because the metallic plate is the one with the lowest stiffness and the ceramic plate is the one with the highest stiffness.

Fig. 4 contains the plots of the axial stress $\bar{\sigma}_{11}$ through-the-thickness of the plate for $k = 0$, 1 and 2. Under the application of the sinusoidal loading, the stresses are tensile at the top surface and compressive at the bottom surface. The homogeneous ceramic plate ($k = 0$) yields the maximum compressive {tensile} stress at the bottom {top} surface. These are the metal-rich surfaces for the FG plates ($k = 1$ and 2). Note that for the different volume fraction exponents chosen, the plate corresponding to $k = 2$ yields the maximum compressive {tensile} stress at the bottom {top} surface of the core layer (see Fig. 4a–c). These are the ceramic-rich surfaces in which the ceramic plates experience the minimum compressive or tensile stresses.

In Fig. 5 we have plotted the through-the-thickness distributions of the transverse shear stress $\bar{\sigma}_{13}$ using both the shear deformation theories. The volume fraction exponent of the FG sandwich plate is taken as $k = 2$. The through-the-thickness distributions of $\bar{\sigma}_{13}$ is also plotted for ceramic plate ($k = 0$). The maximum value occurs at a point on the mid-plane of the plate and its magnitude for FG plate is larger than that for homogeneous ceramic plate. As is known, the FSDPT yields a constant value for transverse shear

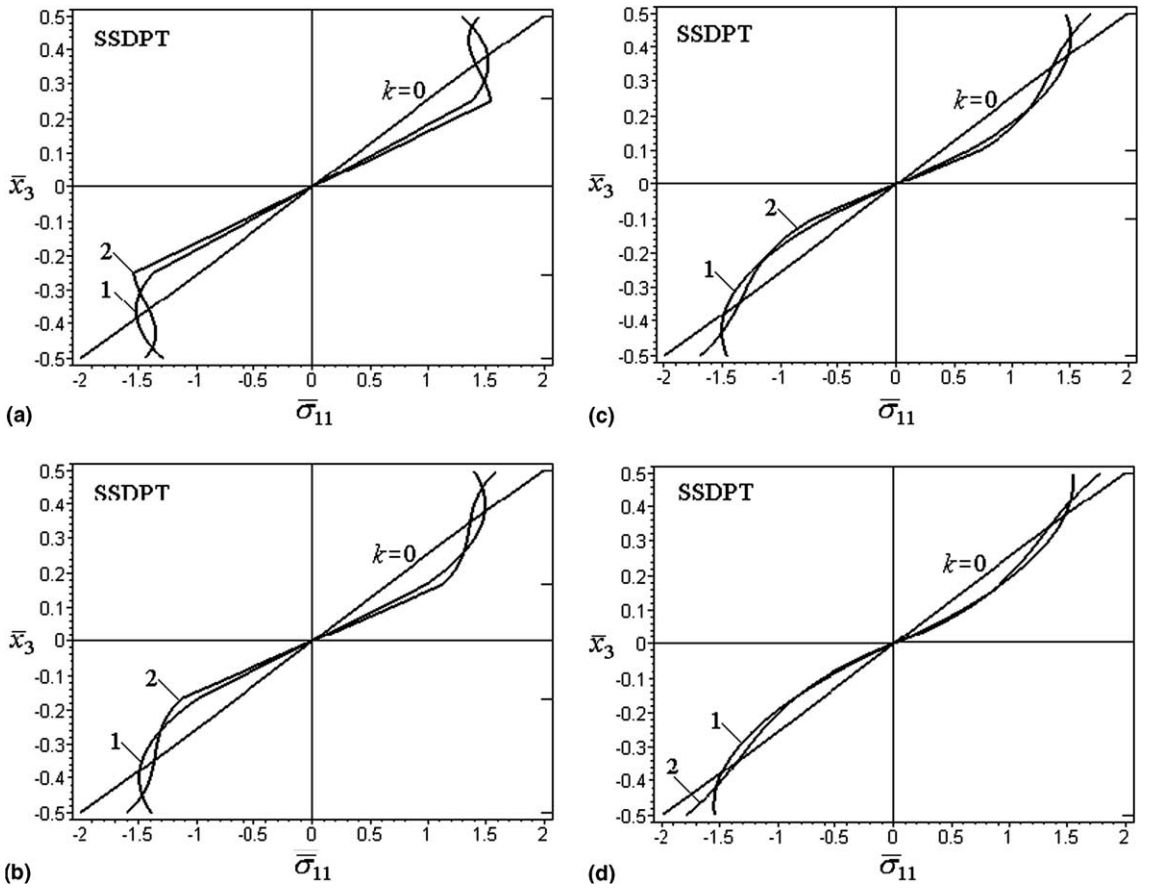

Fig. 4. Variation of normal stress $\bar{\sigma}_{11}$ through plate thickness for various values of the power-law index k and different types of FGM sandwich plates. (a) The (1-2-1) FGM sandwich plate, (b) The (1-1-1) FGM sandwich plate, (c) The (2-1-2) FGM sandwich plate, (d) The (1-0-1) FGM sandwich plate.

stresses of ceramic plate. However, for FG plates it yields values close to that given using TSDPT and SSDPT, especially at the faces of the core layer. The FSDPT could provide more reliable shear stress in the case of (1-0-1) FGM plate (see Fig. 5d).

For the sake of completeness, some results for (2-2-1) FGM sandwich plate are given. Here the plate is not symmetric and the core thickness is the same as one face while it is twice the other. Therefore, in this case we have $h_1 = -h/10$ and $h_2 = 3h/10$. Fig. 6 shows the through-the thickness variation of the volume fraction of the ceramic of (2-2-1) FGM plate for $k = 0.02$, 0.2, 1, 2, 5. In Figs. 7 and 8 we have plotted the through-the-thickness variations of the axial stress and transverse shear stress, respectively. The tensile and compressive values of the axial stress, $\bar{\sigma}_{11}$ (cf. Fig. 7), are maximum at a point on the top surface of the core layer ($k = 2$) and bottom surface of the plate ($k = 0$), respectively. The maximum value of the transverse shear stress, $\bar{\sigma}_{13}$ (cf. Fig. 8), occurs as discussed before at a point on the mid-plane of the plate.

Fig. 9 shows the variation of the non-dimensional center deflection $\bar{u}_3$ with the volume fraction exponent k for the aluminum–alumina and aluminum–zirconia plates. The deflection of zirconia plates is larger than the corresponding one for alumina plates. In general, the deflection increases as k increases and as the core thickness, with respect to the total thickness of the plate, decreases.

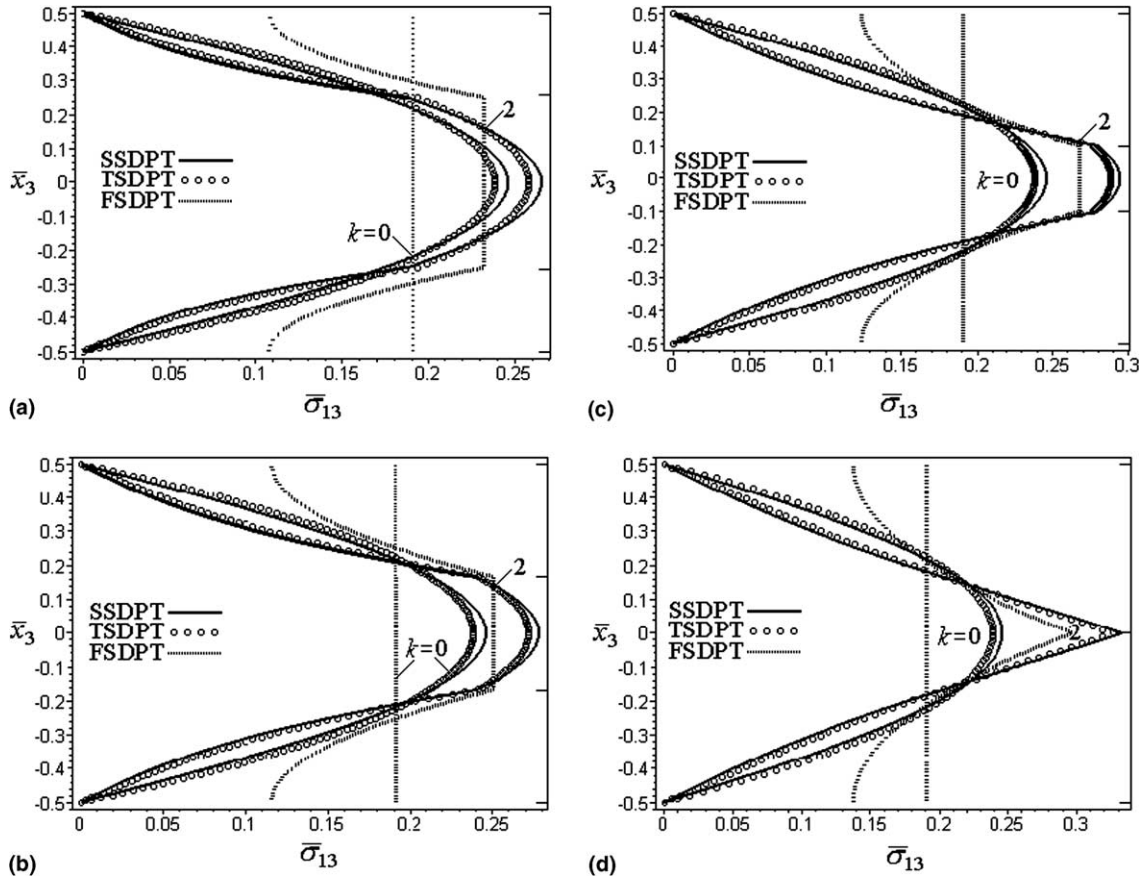

Fig. 5. Variation of transverse shear stress $\bar{\sigma}_{13}$ through plate thickness for different types of FGM sandwich plates. (a) The (1-2-1) FGM sandwich plate, (b) The (1-1-1) FGM sandwich plate, (c) The (2-1-2) FGM sandwich plate, (d) The (1-0-1) FGM sandwich plate.

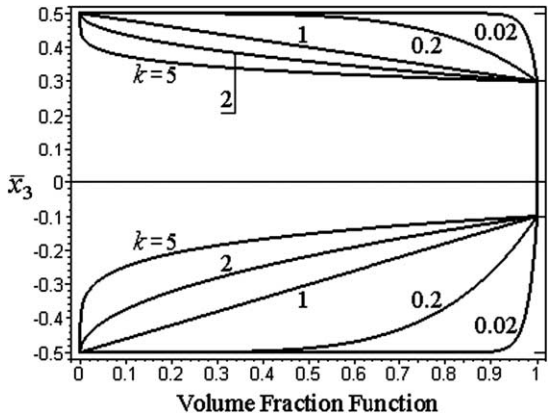

Fig. 6. Variation of volume fraction function through plate thickness of (2-2-1) FGM sandwich plate for various values of the power-law index k.

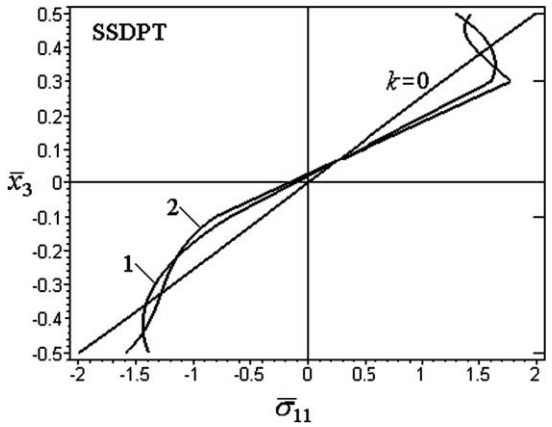

Fig. 7. Variation of normal stress $\bar{\sigma}_{11}$ through plate thickness of the (2-2-1) FGM sandwich plate for various values of the power-law index k.

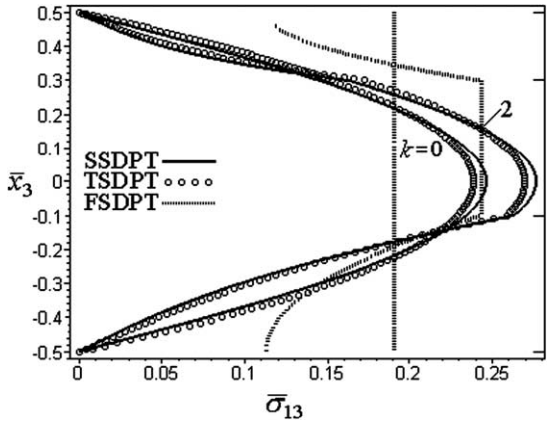

Fig. 8. Variation of transverse shear stress $\bar{\sigma}_{13}$ through plate thickness of the (2-2-1) FGM sandwich plate.

Tables 1–3 list, respectively, values of deflection $\bar{u}_3$, axial stress $\bar{\sigma}_{11}$ and transverse shear stress $\bar{\sigma}_{13}$ for $k = 0$, 1, 2, 5, 10 and different types of sandwich plates. Table 1 shows that the effect of shear deformation is to increase the deflection. The difference between the shear deformation theories is insignificant for fully ceramic plates. It is to be noted that the CLPT yields identical axial stresses with the FSDPT and so Table 2 lacks the results of CLPT. Table 3 shows that the transverse shear stresses as per the FSDPT may be indistinguishable. In general, the fully ceramic plates give the smallest deflections and shear stresses and the largest axial stresses. As the volume fraction exponent increases for FG plates, the deflection, axial stress and shear stress will increase. While these results will decrease as the core thickness, with respect to the total thickness of the plate, increases. In fact the non-symmetric (2-2-1) FGM plate yields the smallest axial stresses.

Finally, the exact maximum deflections of simply supported FGM rectangular plate are compared in Table 4 for different types of FGM sandwich plates ($k = 2$). In addition to the exhibited in Figs. 3 and 9, the deflection will decreases as the aspect ratio a/b increases.

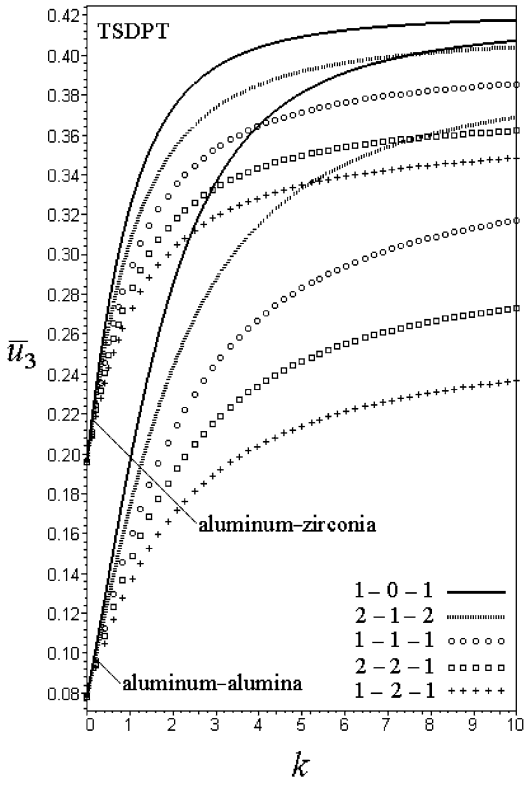

Fig. 9. Dimensionless center deflection ($\bar{u}_3$) as a function of the power-law index k for different types of FGM sandwich plates.

7. Conclusion

A novel type of a three-layer sandwich plate of uniform thickness is developed. Each face is considered as a FG composite material comprised of two distinct material phases, for example, a metal and a ceramic. The gradation of properties through the thickness of the faces is assumed to be of the power-law type. The core is considered as a fully ceramic material. The top and bottom surfaces of the plate are metal-rich while those for the core are ceramic-rich. The static response of FGM sandwich plates is studied according to different plate theories. The stress and displacement response of the plates have been analyzed under sinusoidal loading. The present SSDPT offer accurate and reliable solutions for the analysis of FG plates comparing with other shear deformation theories. Non-dimensional stresses and displacements are computed for plates with two different ceramic–metal mixtures. It is seen that the basic response of the plates that correspond to properties intermediate to that of the metal and ceramic, is necessarily lie in between that of ceramic and metal. The axial stress is found to reach a minimum at a volume fraction exponent that depends on the properties of the constituents. However, the deflection and transverse shear stress are minimums for the fully ceramic plates. Thus, the gradients in material properties play an important role in determining the response of the FGM plates. The present mixture of ceramic and metal with a continuously varying volume fraction can be easily manufactured. This eliminates interface problems of composite materials and thus the stress distributions are smooth.

Appendix A

The elements of the symmetric matrix $[L]$ are given according the different theories by:

SSDPT and TSDPT:

$$L^{11} = -\left(A^{11}\lambda^2 + \frac{1}{2}B^{11}\mu^2\right), \quad L^{12} = -\lambda\mu\left(A^{11} - \frac{1}{2}B^{11}\right), \quad L^{13} = \lambda A^{12}(\lambda^2+\mu^2),$$

$$L^{14} = -\left(A^{13}\lambda^2 + \frac{1}{2}B^{13}\mu^2\right), \quad L^{15} = -\lambda\mu\left(A^{13} - \frac{1}{2}B^{13}\right), \quad L^{22} = -\left(A^{11}\mu^2 + \frac{1}{2}B^{11}\lambda^2\right),$$

$$L^{23} = \mu A^{12}(\lambda^2+\mu^2), \quad L^{24} = L^{15}, \quad L^{25} = -\left(A^{13}\mu^2 + \frac{1}{2}B^{13}\lambda^2\right), \quad L^{33} = -A^{22}(\lambda^2+\mu^2)^2,$$

$$L^{34} = \lambda A^{23}(\lambda^2+\mu^2), \quad L^{35} = \mu A^{23}(\lambda^2+\mu^2), \quad L^{44} = -\left(A^{33}\lambda^2 + \frac{1}{2}B^{33}\mu^2\right) - C,$$

$$L^{45} = -\lambda\mu\left(A^{33} - \frac{1}{2}B^{33}\right), \quad L^{55} = -\left(A^{33}\mu^2 + \frac{1}{2}B^{33}\lambda^2\right) - C.$$

FSDPT:

$$L^{11} = -\left(A^{11}\lambda^2 + \frac{1}{2}B^{11}\mu^2\right), \quad L^{12} = -\lambda\mu\left(A^{11} - \frac{1}{2}B^{11}\right), \quad L^{13} = \lambda A^{12}(\lambda^2+\mu^2),$$

$$L^{14} = -\left(A^{12}\lambda^2 + \frac{1}{2}B^{12}\mu^2\right), \quad L^{15} = -\lambda\mu\left(A^{12} - \frac{1}{2}B^{12}\right), \quad L^{22} = -\left(A^{11}\mu^2 + \frac{1}{2}B^{11}\lambda^2\right),$$

$$L^{23} = \mu A^{12}(\lambda^2+\mu^2), \quad L^{24} = L^{15}, \quad L^{25} = -\left(A^{12}\mu^2 + \frac{1}{2}B^{12}\lambda^2\right), \quad L^{33} = -A^{22}(\lambda^2+\mu^2)^2,$$

$$L^{34} = \lambda A^{22}(\lambda^2+\mu^2), \quad L^{35} = \mu A^{22}(\lambda^2+\mu^2), \quad L^{44} = -\left(A^{22}\lambda^2 + \frac{1}{2}B^{22}\mu^2\right) - C_F,$$

$$L^{45} = -\lambda\mu\left(A^{22} - \frac{1}{2}B^{22}\right), \quad L^{55} = -\left(A^{22}\mu^2 + \frac{1}{2}B^{22}\lambda^2\right) - C_F.$$

CLPT:

$$L^{11} = -\left(A^{11}\lambda^2 + \frac{1}{2}B^{11}\mu^2\right), \quad L^{12} = -\lambda\mu\left(A^{11} - \frac{1}{2}B^{11}\right), \quad L^{13} = \lambda A^{12}(\lambda^2+\mu^2),$$

$$L^{22} = -\left(A^{11}\mu^2 + \frac{1}{2}B^{11}\lambda^2\right), \quad L^{23} = \mu A^{12}(\lambda^2+\mu^2), \quad L^{33} = -A^{22}(\lambda^2+\mu^2)^2.$$

References

Cheng, Z.Q., Batra, R.C., 2000a. Deflection relationships between the homogeneous Kirchhoff plate theory and different functionally graded plate theories. Archives of Mechanics 52, 143–158.

Cheng, Z.Q., Batra, R.C., 2000b. Exact correspondence between eigenvalues of membranes and functionally graded simply supported polygonal plates. Journal of Sound and Vibration 229, 879–895.

Cheng, Z.Q., Batra, R.C., 2000c. Three-dimensional thermoelastic deformations of a functionally graded elliptic plate. Composites: Part B 31, 97–106.

Fukui, Y., Yamanaka, N., 1992. Elastic analysis for thick-walled tubes of functionally graded material subjected to internal pressure. International Journal of Japan Society of Mechanical Engineers, Series A 35, 379–385.

Fukui, Y., Yamanaka, Y., Wakashima, K., 1993. The stress and strains in a thick-walled tube of functionally graded materials under uniform thermal loading. International Journal of Japan Society of Mechanical Engineers, Series A 36, 156–162.

Jin, Z.-H., Batra, R.C., 1996. Some basic fracture mechanics concepts in functionally graded materials. Journal of Mechanics and Physics of Solids 44, 1221–1235.

Koizumi, M., 1993. The concept of FGM. Ceramic Transactions, Functionally Gradient Materials 34, 3–10.

Lee, P.C.Y., Yu, J.D., 1998. Governing equations for a piezoelectric plate with graded properties across the thickness. IEEE Transactions on Ultrasonics, Ferroelastics, and Frequency Control 45, 236–250.

Lee, P.C.Y., Yu, J.D., Shih, W.H., 1999. Piezoelectric ceramic disks with thickness graded material properties. IEEE Transactions on Ultrasonics, Ferroelastics, and Frequency Control 46, 205–215.

Loy, C.T., Lam, K.Y., Reddy, J.N., 1999. Vibration of functionally graded cylindrical shells. International Journal of Mechanical Sciences 41, 309–324.

Noda, N., Jin, Z.H., 1993. Thermal stress intensity factors for a crack in a strip of a functionally gradient material. International Journal of Solids and Structures 30, 1039–1056.

Obata, Y., Noda, N., 1993. Transient thermal stress in a plate of functionally gradient materials. Ceramic Transactions, Functionally Gradient Materials 34, 403–410.

Obata, Y., Noda, N., 1994. Steady thermal stresses in a hollow circular cylinder and a hollow sphere of a functionally gradient material. Journal of Thermal Stresses 17, 471–488.

Obata, Y., Noda, N., Tsuji, T., 1992. Steady thermal stresses in a functionally gradient material plate. Transaction of JSME 58, 1689–1695.

Praveen, G.N., Reddy, J.N., 1998. Nonlinear transient thermoelastic analysis of functionally graded ceramic–metal plates. International Journal of Solids and Structures 35, 4457–4476.

Reiter, T., Dvorak, G.J., Tvergaard, V., 1997. Micromechanical models for graded composite materials. Journal of the Mechanics and Physics of Solids 45, 1281–1302.

Reiter, T., Dvorak, G.J., 1998. Micromechanical models for graded composite materials: II. Thermomechanical loading. Journal of the Mechanics and Physics of Solids 46, 1655–1673.

Reddy, J.N., Chin, C.D., 1998. Thermomechanical analysis of functionally graded cylinders and plates. Journal of Thermal Stresses 21, 593–626.

Reddy, J.N., 2000. Analysis of functionally graded plates. International Journal for Numerical Methods in Engineering 47, 663–684.

Vel, S.S., Batra, R.C., 2002. Exact solution for thermoelastic deformations of functionally graded thick rectangular plates. AIAA Journal 40, 1421–1433.

Yamanouchi, M., Koizumi, M., Hirai, T., Shiota, I., 1990. In: Proceeding of the first international symposium on functionally gradient materials. Sendai, Japan.

Zenkour, A.M., 1999. Transverse shear and normal deformation theory for bending analysis of laminated and sandwich elastic beams. Mechanics of Composite Materials and Structures 6, 267–283.

Zenkour, A.M., 2004a. Thermal effects on the bending response of fiber-reinforced viscoelastic composite plates using a sinusoidal shear deformation theory. Acta Mechanica 171, 171–187.

Zenkour, A.M., 2004b. Analytical solution for bending of cross-ply laminated plates under thermomechanical loading. Composite Structures 65, 367–379.

Zenkour, A.M., 2004c. Buckling of fiber-reinforced viscoelastic composite plates using various plate theories. Journal of Engineering Mathematics 50, 75–93.

Zenkour, A.M., 2005. Generalized shear deformation theory for bending analysis of functionally graded plates. Applied Mathematical Modelling, in press.